Tire/Road Friction Prediction: Introduction a Simplified Numerical Tool based on Contact Modelling

Malal KANE [a], Vikki EDMONDSON [b]

[a] Université Gustave Eiffel
Campus de Nantes
AME/EASE
Allée des Ponts et Chaussées - CS 500444344 Bouguenais
Cedex - France

[b] Northumbria University
Civil Engineering, Engineering & Environment
Newcastle upon Tyne
NE1 8ST, United Kingdom

1. ABSTRACT

The present paper introduces a numerical tire/road friction prediction tool based on modeling the tire/road contact as dynamic, viscoelastic, rough, and lubricated. The tool takes into account a considerable part of influent parameters related to tire, road, contaminant, and contact operating conditions:

- For the tire, the tool takes into account its geometry (width, rim diameter, tread pattern, and depth, etc.), the inflation pressure, and the rubber material behavior (viscoelasticity).
- For the road, the texture is taken into account via the surface topography.
- At the contact interface, dry or wet conditions are taken into account through the lubricant depth, viscosity, and density.
- The operating conditions are taken into account through the normal load, speed, and slip ratio of the tire.

The real novelty of this tool lies in its contact modeling base and its ability to reproduce the complete curve of the tire/road friction coefficient as a function of the slip rate, based on directly measurable parameters such as pavement profile, water thickness, tire radius, etc. in contrast to several models where the input parameters are often indirectly related to the contact actors (the pavement, the tire, and the contact conditions).

The validation of the tool is initially done through parametric studies by analyzing the trends of the results, then by performing braking tests on a passenger car at various speeds on different wet roads with different textures. The tool correctly ranks the ABS (peak friction) and the locked-wheel (sliding friction) tire/road friction coefficient on these various road surfaces.

2. KEYWORDS

Tire/road friction, texture, wet, viscoelastic, rubber, contact, slip ratio, speed

3. INTRODUCTION

Sufficient tire/road friction enables drivers to shorten stopping distances and to follow desired trajectories on roads. Therefore, modeling it remains paramount for tire industries, car manufacturers, and road builders. Indeed, a prediction friction tool may help during the optimization stage of pavement textures and tire materials and can also be set up onboard autonomous vehicles to support adapting their braking.

a. Basic mechanisms

Adhesion and hysteresis are the main mechanisms involved in the generation of friction [1]. The adhesion occurs when local bonds form between the tire tread and the road. The movement of the tire causes these bonds to continually stretch, rupture, and renew [2]. The hysteresis comes from the damping in the tire tread rubber material as it deforms when it passes over the road surface asperities by opposing movement upstream of the asperities and recovering its shape downstream [3-5]. To be effective, adhesion requires close contact between the two involved surfaces and thus clean and dry surfaces, while the hysteresis requires local cyclic local deformations of the tire tread and thus rough surfaces [2, 6-8].

b. Influencing factors

The friction is then influenced as much by the two first bodies in contact (the tire and the road) and the third body between them (contaminant) as by the contact operating conditions.

Road surface Texture

The mechanisms governing the hysteresis showed how important the asperities at the road surface[1] are in the generation of the friction forces. The set of these asperities is commonly named "Texture" and is often divided into two scales named "Macrotexture" and "Microtexture" [9]: The macrotexture is of the same order as the road surface aggregates with wavelengths and peak amplitudes of [0.5 to 50 mm] and [0.1 to 20 mm] ranges respectively. The microtexture can be felt in terms of the harshness of the surface and is constituted by all wavelengths less than 0.5 mm and having peak amplitudes of [0.001 - 0.5 mm].

Many investigations have been undertaken to determine the role of these two texture scales. Sabey's tests showed that in wet conditions at low speeds higher Microtexture benefits friction, and higher speeds, lower Macrotexture disadvantages friction [10]. Many empirical models have been proposed too to determine the role of these scales [11, 12]. One can consider the International Friction Index (IFI) and the Penn State model derived from statistical fittings of measured tire/road friction data [13, 14]. These models represent the graphical curve of the friction versus speed through equations with two parameters, where the first is the intercept, occurring at zero vehicle speed, and is related to the microtexture. The higher the microtexture, the higher the intercept will be. Whilst the second parameter describes the slope of the curve and is related to the macrotexture. The smaller the macrotexture, the faster the curve drops.

[1] In order not to make the text heavier, the term "Surface" will be used instead of "road surface" in the rest of the document.

Tire

The tread, the part of the tire in contact with the road, has several particular aspects that influence friction. Beyond the effect of the viscoelasticity of its material on the hysteresis, the role of the tread pattern is extremely important too, particularly on low macrotextured surfaces. Indeed, it negates the lack of macrotexture by providing channels from which water can escape at higher speeds [15].

Contact conditions

The contaminants present on the surface may separate the tire from the road. Indeed, in the case of wet surfaces, an increase in tire speed may separate it partially from the surface, where the hydrodynamic pressure created in the water trapped in the contact balances a part of the normal load. In this extreme situation, the tire is effectively lifted off the road and all grip and steering control are lost [16].

Operating conditions

At a given speed, the friction increases with the slip ratio until a peak value, commonly known as "peak friction". Peak friction typically occurs between 10 and 30% slip ratio. After the friction starts to decrease until 100% of slip ratio, commonly named "sliding friction". The magnitude of the peak and sliding frictions will depend on the contact conditions, tire characteristics, surface texture, and vehicle speed.

On the other hand, for a given slip rate, friction tends to decrease with speed on wet surfaces. This decay rate will greatly depend on the macrotexture (as outlined above) [10].

c. State of the art about modeling

Empirical

Many empirical (but practical) formulae have been proposed relating the operating conditions to the friction [17-19]. The most famous is Pacejka's, often termed the "Magic Formula" [20]. Whilst this formula reproduces the friction curve as a function of the slip ratio, it has too many coefficients to be identified from experiments. Therefore, the limitation of such models is the assignment of values to calibration coefficients that have to be identified from experiments.

Physical

Finite-elements based models have been introduced too. Such models are very cumbersome in terms of calculation time and parameterization, making them tough to use [21].

It exists simpler models considering the friction forces as resulting from the tire tread deformations and therefore depending on its stiffness. The most usual approach is to consider the tread as a brush, with each bristle attached to the road surface being wrinkled to a certain limit with the movement of the tire [21, 23]. Each author proposes his law of deformation for the bristles more or less complex, with often some parameters to be determined empirically or after correlation with experimental results.

There are also physical models coupling fractal considerations of the surface texture and contact modeling to estimate the friction. Persson developed a fractal-based friction model after showing the achievability of scales-independent description of the texture [24, 25]. From a contact model, he explored the relationship between the real contact area and the friction. Recently, Villani et al., inspired by Heinrich's work [4], calculated the hysteresis contribution through an analytical model of a sliding rubber over surfaces described with fractal dimension and upper cut-off length [5].

These approaches, constructed from solid physical bases, are very complex to use since many coefficients accompanying them remain very difficult to determine. To overcome this complexity, new simpler approaches based on deterministic modeling of the contact started emerging [26].

Contribution of this present work

The present work is in line with these emerging approaches [26]. It introduces a friction prediction tool based on deterministic modeling of the tire/road contact as dynamic, viscoelastic, rough, and lubricated contact. The tool takes into account almost all parameters related to tire, road, contaminant, and contact operating conditions. For the tire, the tool takes into account its geometry, inflation pressure, and rubber material. For the road, the texture is taken into account via its profiles. At the contact interface, dry or wet conditions are accounted via the lubricant depth, viscosity, and density. The operating conditions are taken into account via the normal load, speed, and slip ratio of the moving tire.

In the rest of the document, the modeling basics behind the tool will be presented and concluded by the algorithm behind the tool. The experimental setup to validate the tool will be detailed. Two parts dedicated to the validation of the tool will follow. The first part will be devoted to the analysis of the trends of different simulation results of the tool resulting from parametric studies, then the second part will be devoted to the comparison between the experimental results and those of the tool.

4. THE TOOL

a. Modeling

The concept behind

The tool is based on the calculation of the friction generated in the wet contact path between a rotating tire on a rough road surface with a given speed and slip ratio. Note that only 2D contacts are considered without taking into account the asymmetrical pressure distribution within the contact patch. The fiction is assumed to originate from hysteresis and adhesion, perturbed by the hydrodynamic effect of a lubricant [26]. The hysteresis contribution is evaluated from the envelopment dissymmetry of the surface asperities by the moving viscoelastic tire tread. The actual adhesion contribution is considered negligible in wet conditions. But, to take into account the "local" roughness (corresponding to scales smaller than the resolution at which the texture is captured), a "local" contribution similar to an adhesion coefficient is introduced into the formulations (See next section) [26]. The calculation procedure is completed in two steps:

- The first step is to determine the global deformation of the loaded tire and thus the apparent contact area. This step is complete at the scale of the tire structure, and in static mode by considering the road surface as smooth and rigid. The inputs at this stage are the tire diameter, the normal load, and an "equivalent structural stiffness"[2] (related to the inflation pressure and the carcass stiffness of the tire) and by neglecting the stiffness of tread (Figure 1 (a)). Note that this static approach of the tire to estimate the apparent contact area remains a simplification. Indeed, when a slip rate is introduced, the movement of the tire will imply a different dynamic radius than a static one, and thus there is a slight difference between the apparent areas. However, the simplification introduced at this stage will avoid a supplementary loop between this step and the one below which would lead to much more complex and time-consuming calculations. It can be justified by the fact that only what happening in the contact area is of interest and not the overall tire dynamic behavior. The calculation details of this global deformation of the loaded tire are detailed in the "Calculation Algorithm" section.
- The second step is to coat the deformed tire above with its grooved tread of rubber material, and afterward, move the whole upon the rough road surface. At this calculation stage, the input parameters include the load, the rubber behavior law, the speed, and the slip ratio of

[2] In order not to make the text heavier, the term "Carcass stiffness " is often used instead of " equivalent structural stiffness " in the the document.

the tire, the surface topography, the water thickness … (Figure 1 (b)). The calculation of the friction will be detailed in the next section.

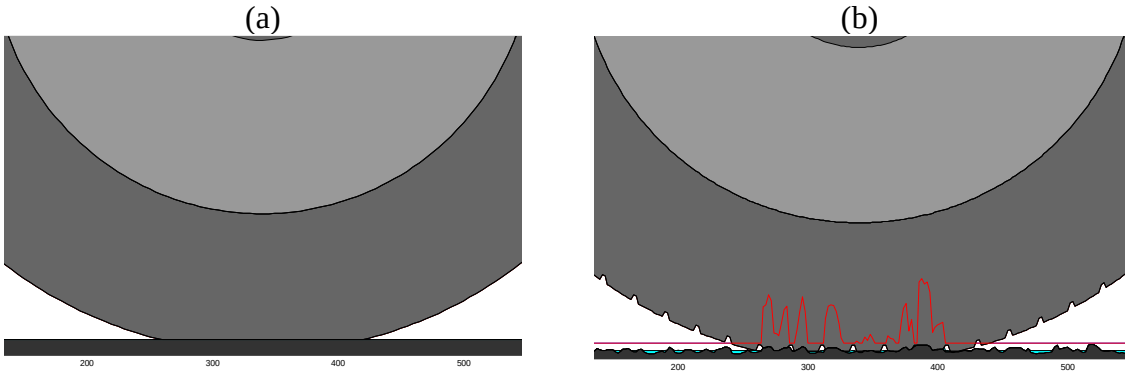

Figure 1: The two calculation steps. The first determines the apparent contact area assuming the tire static and the road smooth (a). The second step determines the real contact area and thus the friction with the moving tire tread patterned on the rough road surface (b).

Calculating the friction

The governing equations (Equations 1 to 8) are derived from the balance of the forces acting in the contact area [26]. The index i and j localize respectively a tread element and a road element. For an i^{th} moving tread element in contact with j^{th} static road element, Equation 1 traduces the equilibrium of the forces (Figure 2).

$$\overrightarrow{F_{ij}} + \overrightarrow{T_{ij}} + \overrightarrow{R_{ij}} + \overrightarrow{FR_{ij}} = \vec{0} \qquad \text{Equation 1}$$

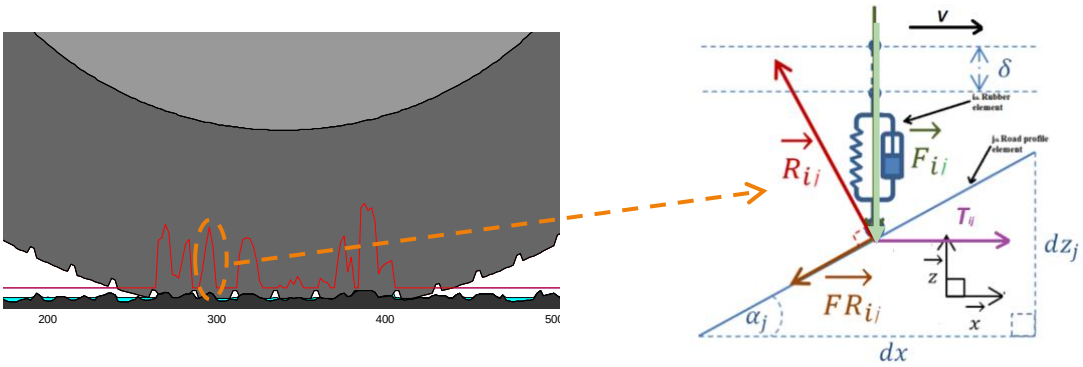

Figure 2: Forces acting between rubber and road profile elements

Where,

- $\overrightarrow{F_{ij}}$ is the local contact force applied by the rubber element on the surface element. In the present work, a "Kelvin-Voigt" model is used for the rubber, where K is the spring's stiffness per unit length and C is the dashpot's viscosity per unit length. $\overrightarrow{F_{ij}}$ is balanced by the load through the contact pressure p_{ij}.
  - $F_{ij}(t) = l \times dx \times p_{ij}(t)$ with $p_{ij}(t) = Ku_{ij}(t) + C\frac{du_{ij}(t)}{dt}$ and $u_{ij}(t) = \delta(t) - h_i + z_j$
  - With, t representing the time and dt being the time that a rubber element i moves from point j to j+1 of the road surface (dt = dx/V, where V is the slip speed of the element i). $u_{ij}(t)$ the displacement of the tread i^{th} element contacting j^{th} element on the road at time t. $\delta(t)$ is the solid displacement of the tire at t. h_i represents the tire geometry. z_j is the height of the j^{th} point of the road profile.
- $\overrightarrow{T_{ij}}$ is the traction force. This force must be equal or just greater than the friction force opposing the movement.
- $\overrightarrow{R_{ij}}$ is the normal surface reaction force.
- $\overrightarrow{FR_{ij}}$ is a local friction force. $FR_{ij} = \mu_{\mathbf{loc}} R_{ij}$ when the element is moving on a "pseudo smooth inclined plan" with angle α_j . $\mu_{\mathbf{loc}}$ represents a local friction coefficient corresponding to the actual adhesion coefficient (that is nil in the wet) and/or a local hysteresis coefficient accounting the contribution of the asperities witch the wavelength is smaller than the resolution with which the surface texture is captured. Figure 3 illustrates the multiscale representation of the local scale from larger to smaller resolutions [24].

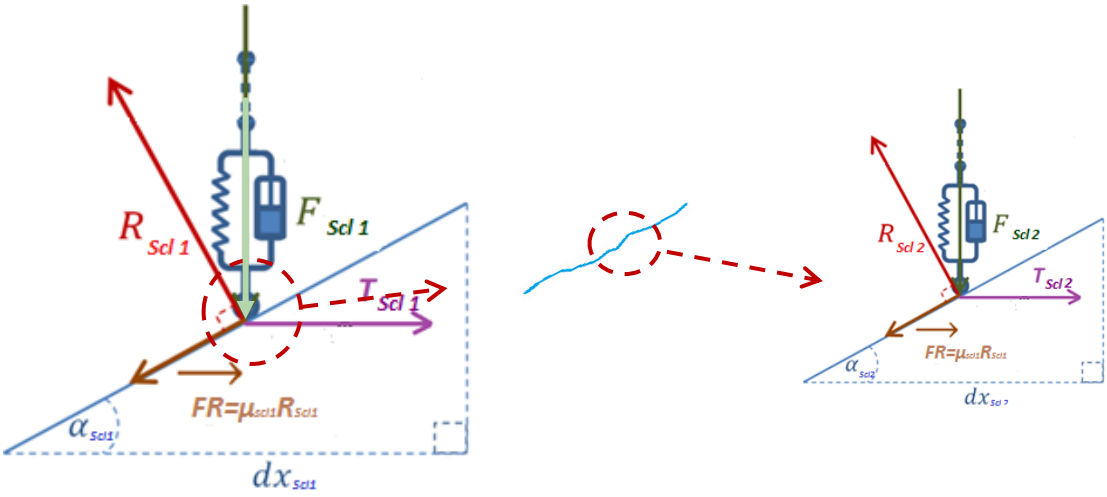

Figure 3: Fractal representation of the local hysteretic contribution of all texture scales smaller than the resolution with which the profile is recorded- From left to right, larger to finer scales (here, scales 0 to 2 are illustrated)

The projection of Equation 1 onto axes x and z, coupled with the condition that $FR_{ij} = \mu_{loc} R_{ij}$ leads to:

$$T_{ij}(t) = F_{ij}(t) \frac{\sin(\alpha_j) + \mu_{loc} \cos(\alpha_j)}{\cos(\alpha_j) - \mu_{loc} \sin(\alpha_j)} \quad \text{Equation 2}$$

When a tread element is not in contact with the road surface, its contact pressure is nil and the element is subjected to a relaxation phase. Its position on the Z-axis is then determined by solving this:

$$Ku_{ij}(t) + C \frac{du_{ij}(t)}{dt} = 0 \quad \text{Equation 3}$$

At any time t the total load W applied by the tire on the road surface must be balanced by the normal contact pressure:

$$W = \sum_i^N F_{ij}(t) \quad \text{Equation 4}$$

Where,

N is the number of elements comprising the tire tread in the contact area. Accordingly, the global friction coefficient $\mu_j(t)$ can then be calculated using the following formula:

$$\mu_j(t) = \frac{\sum_i^N T_{ij}(t)}{W} \quad \text{Equation 5}$$

At this stage, the only unknown factors are $F_{ij}(t)$, representing the distribution of the contact forces applied by the tread to the road surface. For the calculation details, the reader is advised to referrer to the following publications [26].

Introducing the slip rate

The slip rate τ is introduced during the rotation of the tire via the relative positioning of the rubber and road elements. Assuming the tire moving on the surface at speed V and a slip ratio τ. If at t, the rubber element i^{th} is in contact with the road element j^{th}, at t+dt, the position of the rubber element i^{th} would be:

$$i = j + \left\lfloor \tau \times V \frac{dt}{dx} \right\rfloor \quad \text{Equation 6}$$

Lubricating the contact (wetting)

Additionally, depending on the operating conditions a hydrodynamic pressure will be generated in the water trapped between the tire tread and the road surface. This hydrodynamic

pressure exerts a lift up force on the tread and thus decreases its penetration depth in road asperities. To take into account this phenomenon, a "pseudo hydrodynamic bearing" simplification is adopted by calculating its "hydrodynamic bearing capacity" W_h.

Note that this approach remains an extreme simplification. Indeed, it does not account for the flow of the fluid in the contact area. Indeed, under wet conditions, a much stricter coupling would have to be made between the contact equations and the Navier-Stokes equations at each point of the contact area (which would lead to much more complex and time-consuming calculations). For a more respectful physical approach, the reader is invited to see the following work: [27].

$$W_h = \frac{\alpha 6 \eta V^{\beta} l L^2}{H_{out}^2 (a-1)^2} \left[\log(a) - 2\frac{a-1}{a+1} \right] \quad \text{Equation 7}$$

Where, $a = \frac{H_{in}}{H_{out}}$, with H_{out} and H_{in}, are respectively the outlet and inlet water thicknesses of the "pseudo hydrodynamic bearing". η is the water viscosity. L and l are the lengths and the width of the apparent tire/road contact area. α and β are two empirical coefficients (10^5 and 1.75 respectively) added to adjust the load capacity of the "pseudo hydrodynamic bearing". For the calculation details, the reader is invited to refer to the following publication [26].

b. Calculation algorithm

Table 1 summarizes the inputs of the model. These inputs are related to the tire, the road, the contaminant, and the operating conditions. Figure 4 illustrates the algorithm of the numerical calculation program.

Table 1: Inputs of the model

Tire	Road surface	Contaminant	Op. conditions
• Tire dimensions (Width and Diameter) • Tread depth • Carcass stiffness • Rubber characteristics (if Kelvin Voigt model: Stiffness and Viscosity	• Surface profile • Resolution • Adhesion coefficient	• Density • Viscosity • thickness	• Normal load • Speed • Slip ratio

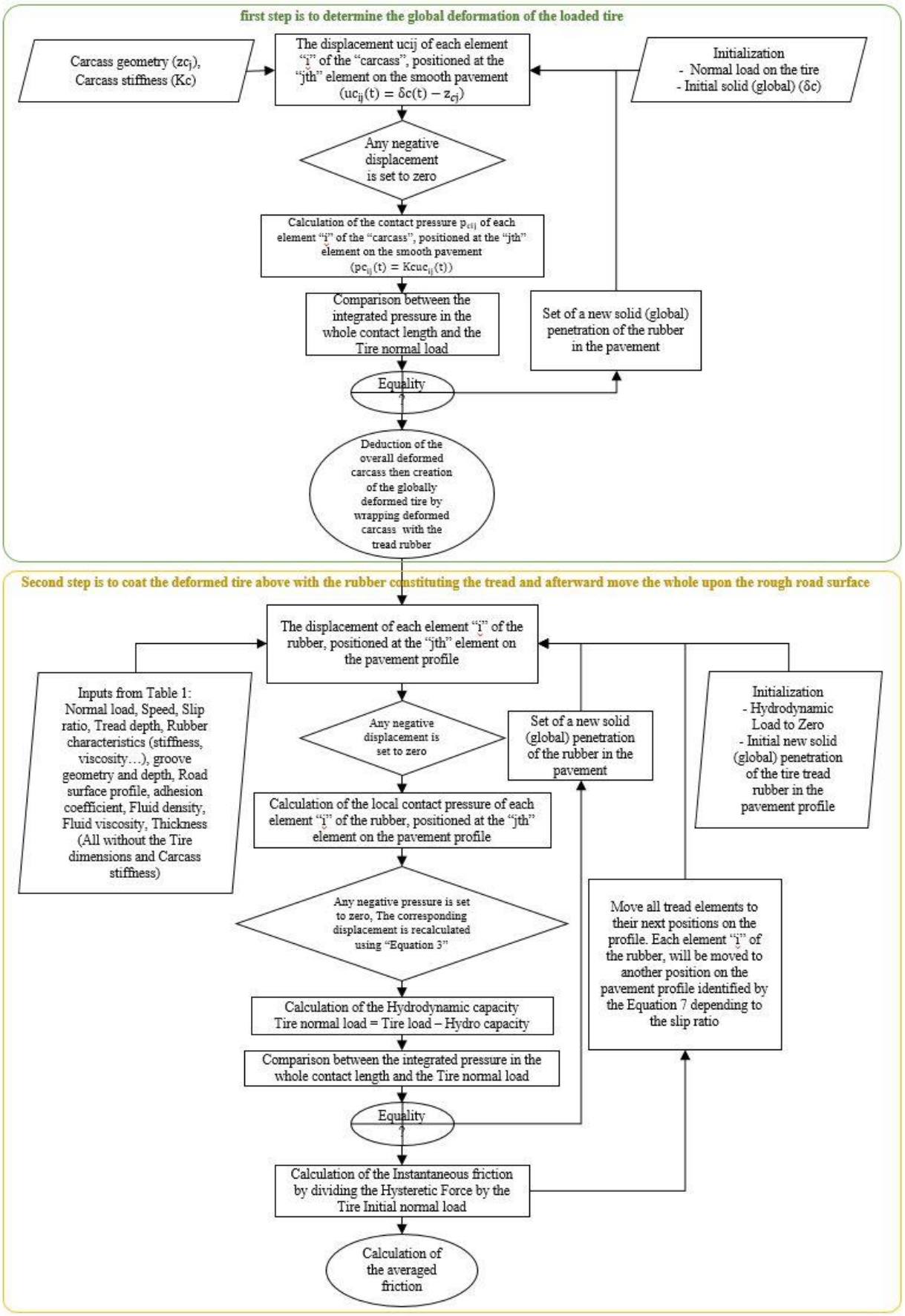

Figure 4: General algorithm for calculating the tire/road friction

c. Road surfaces

The test surfaces are located at the test track of the Gustave Eiffel University in Nantes (western France). They embed many combinations of microtexture and macrotexture scales, providing thus different levels of grip. Figure 5 (a) names and illustrates the surfaces and gives also details of the materials. To input these surfaces in the tool for simulations, their textures are captured using a profilometer (Figure 5 (b)). 12 parallel profiles of 1200 mm length (corresponding to twice the diameter of a regular passenger car tire) with a resolution of 0.1 mm, and regularly distributed across a width of 350 mm (corresponding to the width of a regular passenger car tire) are captured on each surface.

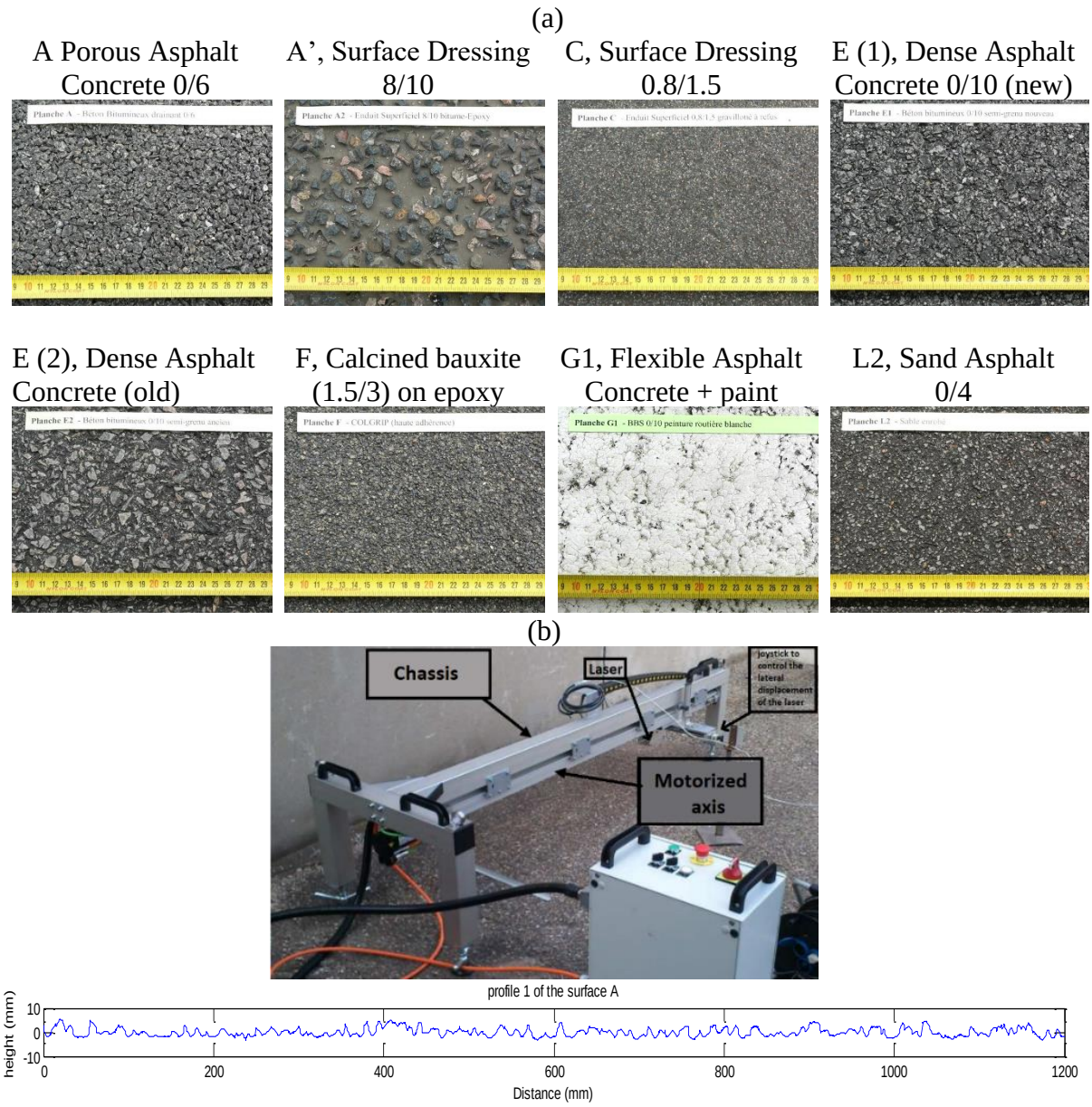

Figure 5: (a) Test surfaces, (b-Up) - System to capture the profiles of the test surfaces, (b-Down) - Example of a captured profile [28]

d. Testing vehicle

The test car is a passenger sedan car, a Clio 3® from Renault® frequently used on European roads (Figure 8). Its characteristics and the main sensors attached to it (needed to capture the inputs to run the tool) are displayed in Table 2 and Figure 6.

Table 2: Car characteristics and the list of main sensors

Car Information	
Model	Renault Clio 3
Weight	1485 kg
Larger	1,72 m
Weight (front wheels)	858 kg
Inflation Pressure (front)	2,2 bars

Sensor	Quantity Measured	Manufacturer
Dynamometric Wheel	Force and Torque	KISTLER
Optical speedometer	Longitudinal speed	CORRSYS DATRON
Encoder	Wheel speed	BAUMER
Water Depth	Water thickness	AQUASENS

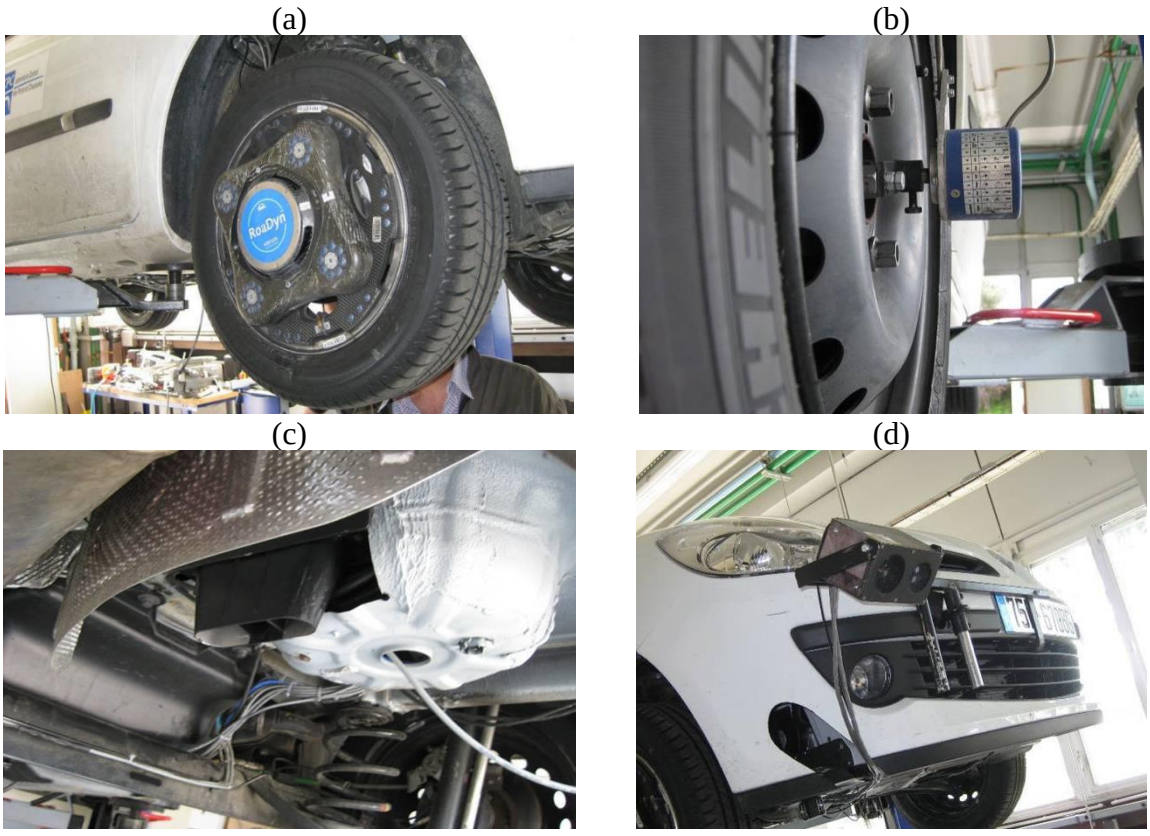

Figure 6: Main sensors attached to the testing car

e. Test tire

To input the tire in the tool for simulations, its geometry is modeled in 2D, represented by a circle with grooves at its circumference of a height equal to the grooves' depth (Figure 9 (a)). The carcass and the tread stiffness need to be determined to run the tool. This is achieved with an experimental setup to load the tire on a road sample Figure 7 (c), to estimate the apparent and real contact areas. The setup consists of a hydraulic cylinder with two arms, the ends connected by a bar passing through the tire axle (Figure 7 (a)). The hydraulic cylinder is connected to a hydraulic pump which, when activated, allows the cylinder to load the tire on the surface.

To determine the apparent and real contact areas, liquid silicone is placed between the tire and the road, and the two are brought into contact (Figure 7 (b)). Once the silicone dried, the tire is unloaded and a photograph of the contact path imprinted on the silicone is taken (Figure 7 (d)) and the apparent and real contact areas are evaluated from it (Figure 7 (e)). Once these contact areas are determined, a back-calculation is made using the tool itself but in static mode to determine the corresponding stiffness (Table 3). A further back-calculation is completed in dynamic mode, with a locked-wheel to determine the rubber viscosity (set to 500 Ns/m in the simulations within this study).

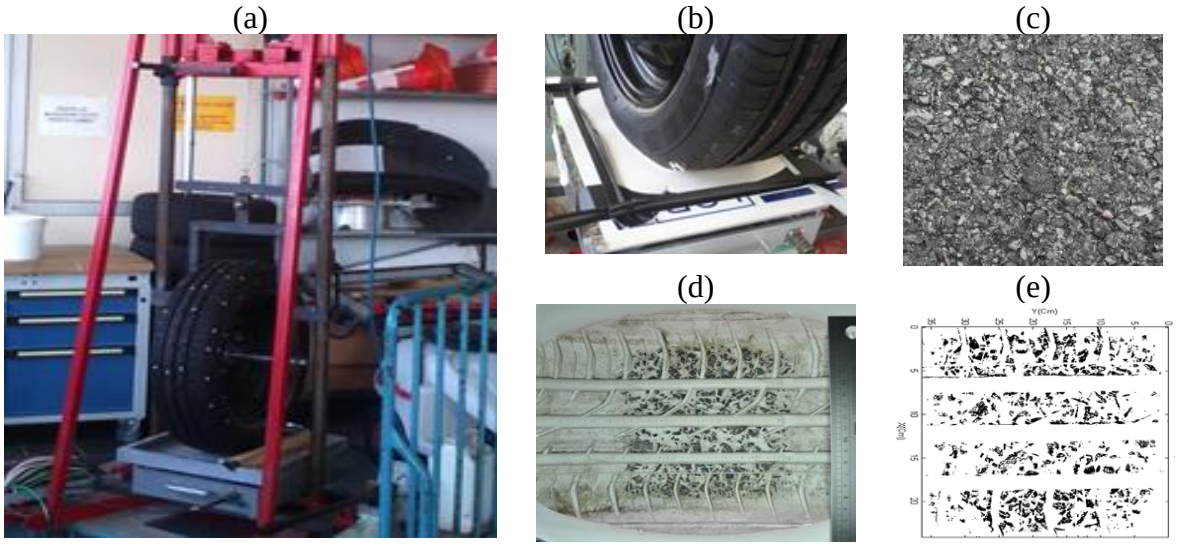

Figure 7: Experimental setup to load the tire on a road sample and estimation of the apparent and real tire/road contact areas

Table 3: Measured tire/road contact dimensions and the estimated tread rubber and carcass stiffness

Contact length (cm)	Contact width (cm)	Apparent contact area (cm^2)	Real contact area (cm^2)	Carcasse stiffness (N/m^3)	Tread rubber stiffness (N/m)
13.28	13.78	183	34.94	41897000	129.56

f. Test procedure

For each test, the procedure below is followed:

- The track is first sprayed with water using a system of nozzles placed all along its length. Watering is stopped when the thickness reaches a target between 1 to 2 mm checked with the VAISALA® sensor (circled in red in Figure 8 (b)) (The actual water thickness varies depending on the surface and the position).
- Then, the watering is stopped and the braking test starts. The test is carried out holding the vehicle speed at 60 km/h (a), and once the car is on the right surface, the driver brakes (b). This sequence is repeated twice, with the ABS on the first run and off the second.

(a)  (b) 

Figure 8: Test procedure - holding the speed, once the car is on the right surface, the driver brakes

6. VALIDATION OF THE TOOL

The validation of the tool is done in two parts. The first part will be devoted to checking the relevancy of the tool by analyzing the trends of different simulation results, then the second part will be devoted to the comparison between the test results and those of the tool.

a. Relevancy of the model

Reproducibility of the model of some the general known trends

Figure 9 displays two different pressure distributions between a patterned tire moving on the surface A (Figure 5 (a)) simulated with the tool. In these two simulations, all inputs are the same except the slip ratio (equal to 0 for Figure 9 (a) and 0.04 Figure 9 (b) respectively). The blue color represents the contaminant (water here).

It can be seen that the increase in the slip speed results in a decrease in the local contact areas[3] and thus in an increase in the pressure peaks. It's like the rubber is getting harder. The

[3] The terms " local contact areas " and " real contact areas " are used indiscriminately in the document.

mechanism behind this phenomenon comes from the fact that the faster the rubber slips on the asperities' upstream side, the less it touches the asperities' opposite side (due to its delayed relaxation), resulting in reduced contact areas and the pressures located more forward of the asperities. This observation is in line with the literature [2].

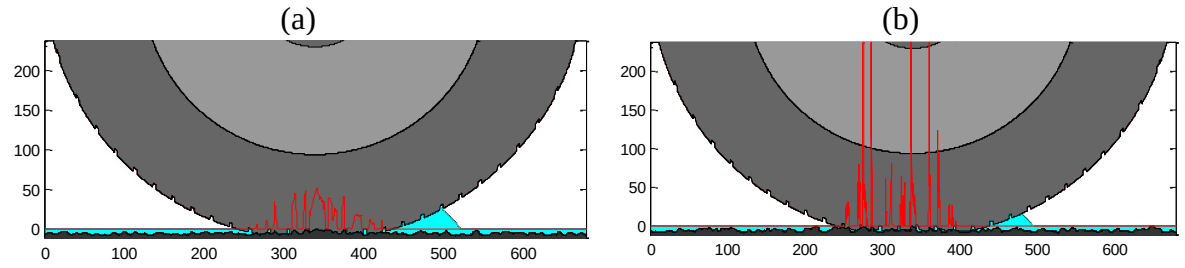

Figure 9: Two different outputs of the model with two different inputs (60 km/h for both, but at different slip ratio: 0 (a) and 0.04 (b) respectively at left and right). The blue color represents the contaminant (water here)

Figure 10 (a) displays a typical 3D plot of experimental results of friction versus slip ratio and speed [29]. The tests were carried out on a flooded (3mm of water depth) surface similar to "A" with 0.9 mm of equivalent texture depth with a high wear PIARC tire loaded at 300 daN [30]. Figure 10 (b) shows results of simulations with the tool with inputs corresponding to the same operating conditions as those of the above experiments (but not the same surface, as we did not have it at our disposal, so we used the profiles of the surface A (Figure 5 (a)).

The two 3D curves show the same trend; the maximum friction coefficient usually located between 10% and 20% of the slip rate and its decline after. The decrease of the friction coefficient with the speed at locked-wheel is also very well reproduced.

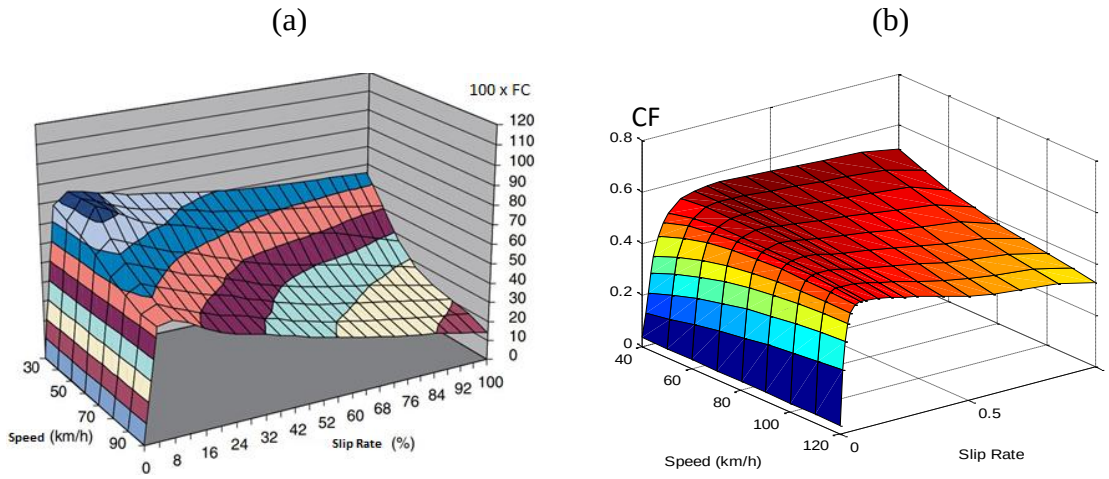

Figure 10: The (a) and (b) display typical examples of tire/road friction coefficient variation against the slip ratio and speed respectively from experimental results [29] and calculated with the model

Effect of texture capture resolution

The effect of the resolution *dx* used to capture the texture (see Figure 2) on the tool predictions is explored in this section. Figure 11 (a) shows the curves of the friction versus slip ratio at different resolutions (dx varying from 100 to 10000 µm) of the same surface (with $\mu_{loc} = 0$, meaning no contribution of actual adhesion or of texture of wavelength below dx).

One observes that the higher the resolution, the higher the friction at any slip ratio (Figure 11 (b), Figure 11 (c). This meaning that higher resolution of the texture will embed more smaller-scales (microtexture) and thus will benefit to friction. This finding is again in agreement with Sabey's results already discussed in the introduction section [10].

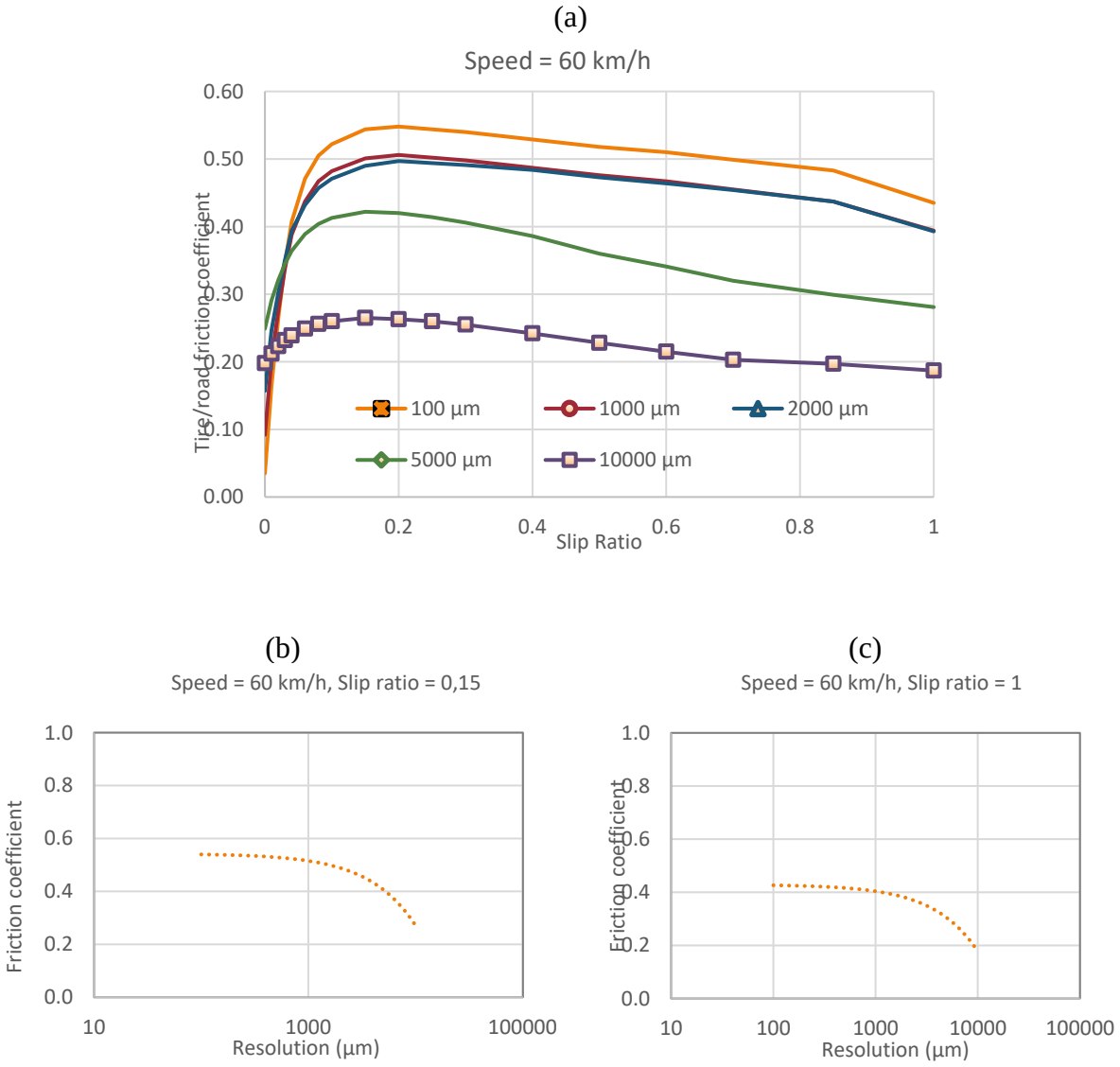

Figure 11: (a) Effect of the road surface resolution - friction coefficient versus slip ratio on the same surface captured at different resolutions. Effect of the resolution on the peak (b) and sliding frictions (c)

Effet of speed and slip ratio

Figure 12 (a) shows predicted friction versus slip ratio at different speeds. The simulations are performed using the profile of the surface A at 100µm resolution and with $\mu_{loc} = 0$.

One sees that as speed increases, the sliding friction decreases, which is again in agreement with Sabey's findings [10]. For the other slip ratios: At 0-slip ratio, the effect of speed on friction is negligible (Figure 12 (b)). Between 0 to 10% slip ratio, the friction increases with speed until the peak-slip ratio is achieved (Figure 12 (c) and (d)). After, the friction coefficient with speed until the sliding friction (Figure 12 (d) and (e)). This illustrates the need to properly adjust the ABS operating slip rate of a vehicle.

(a)

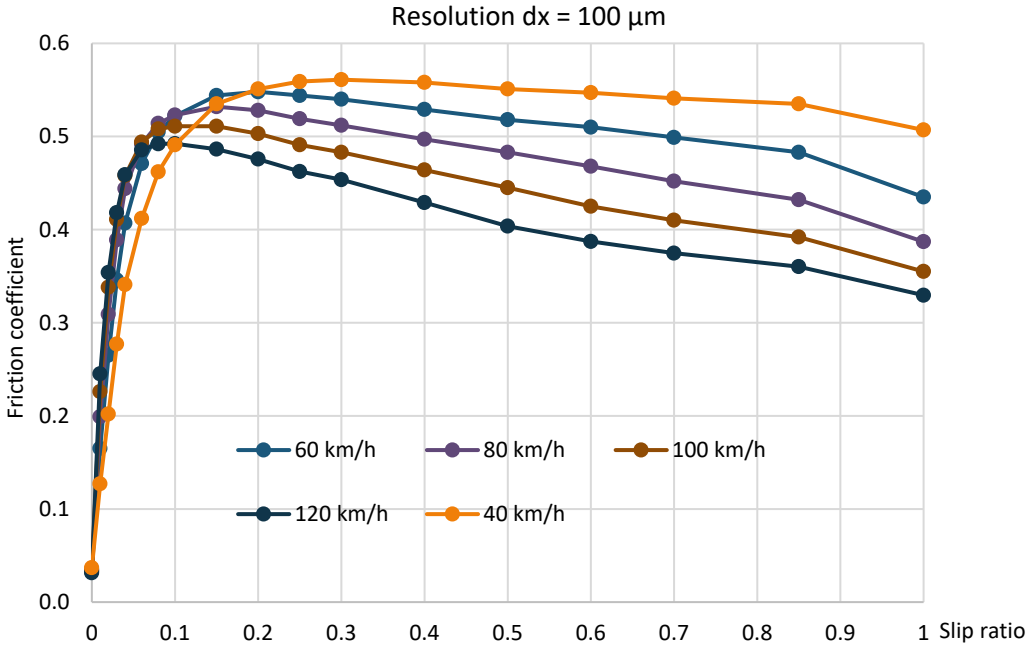

(b)

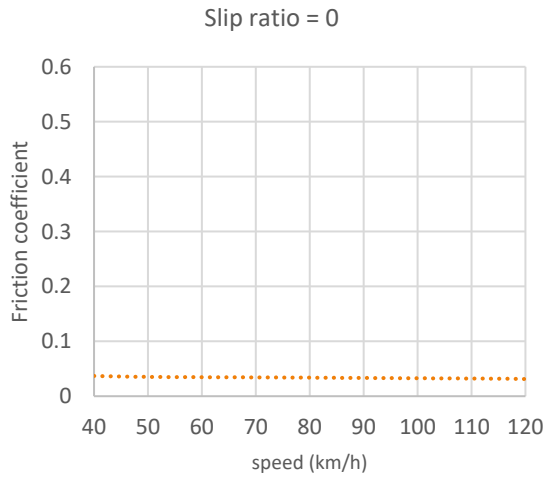

(c)

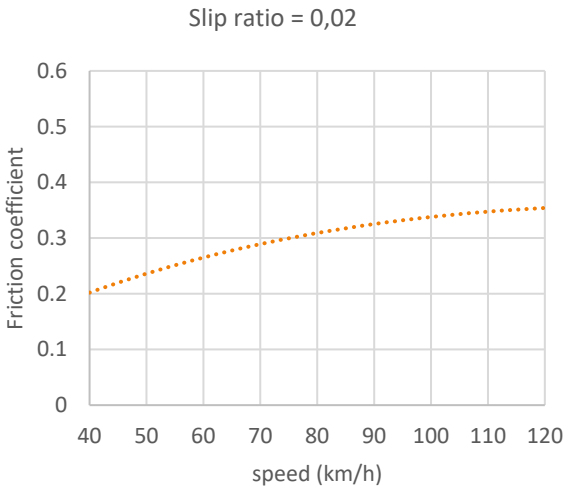

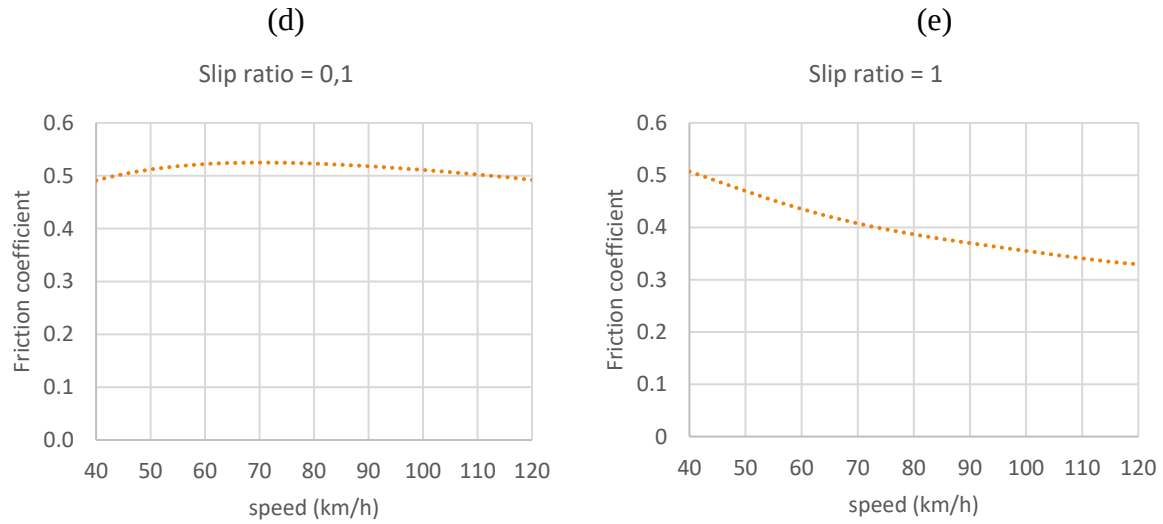

Figure 12: (a) Friction coefficient versus slip rates at different speeds. (b-d) Friction coefficient versus speed at given slip rates

b. Experimental validation - Comparison between infield tests and the tool predictions

The experimental validation is completed by comparing the friction predicted by the tool with infield braking tests. The devices and the test procedure were discussed in the "Experimental device" section. For all surfaces, their profiles used as inputs in the tool to proceed to the simulations are captured with a resolution of 100 µm (The limiting resolution that our system is capable of capturing in-situ).

Figure 13(a) and (b) show the peak-frictions (red bars) and sliding-frictions (green bars) respectively predicted by the tool and by tests on the eight surfaces. Principally, the ranking of the surfaces in terms of peak-frictions and sliding-frictions is the same for both the model and the experiments (except for the sliding-frictions of the surface A), even though the model values are reported at almost 50% of the corresponding experimental values. This inferiority of the model values can be explained by the low capture resolution of the surfaces, which at 100 µm leaves a great part of the microtexture out of the captured profiles. The tendency of the tool to predict less is accentuated for surfaces with higher microtexture (F and A), where a major part of that microtexture is not captured (Figure 13 (c)). Better results from the tool would probably be obtained if the capture resolution of surfaces was increased. However, the current profilometer at our disposal does not allow us to go beyond this resolution.

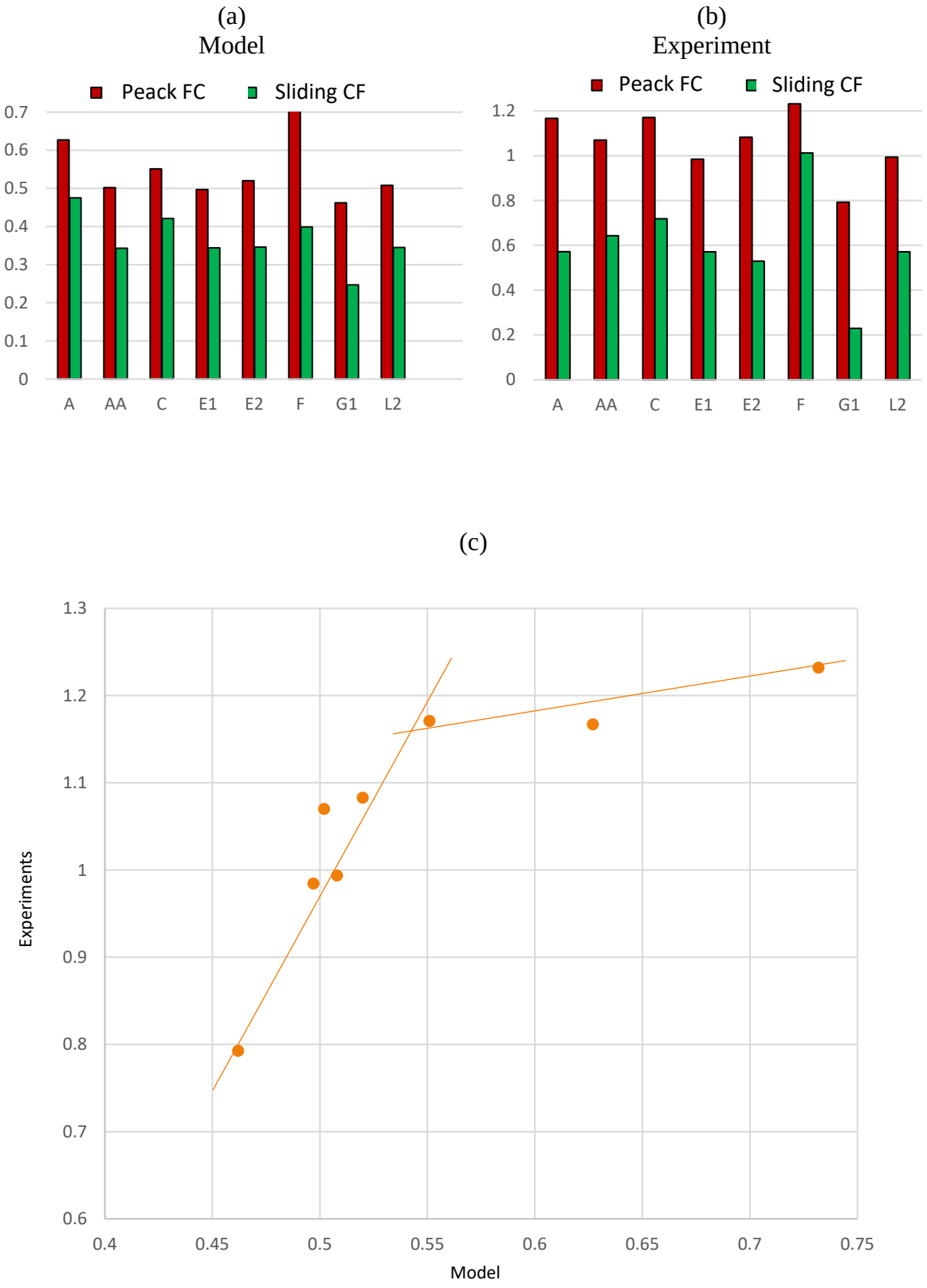

Figure 13: Peak-frictions and sliding-frictions on different test surfaces. (a) - Model (100 µm of surface resolution), (b) - Experiments (Braking tests), (c) - Direct comparison between the experimental and model peak-frictions

d. Discussion

Although the tool offers great prospects in terms of road safety, especially in the prediction of available grip, it turns out that there is still room for improvement:

- One area of improvement would be to know at what resolution to capture road surfaces;
- Or at least, being limited by the capabilities of current in-situ profilometers with which it is impossible to go below the resolution of 100 µm, how can these non-capturable scales be taken into account in the simulations via μ_{loc}.
- The evolution of the tool towards 3D and the more rigorous consideration of water flow are also necessary for future improvements.
- Another challenge would be how to boost the speed of the calculations by simplifying the model as much as possible.

One of the future applications of this tool could be its use onboard autonomous vehicles. Indeed, this tool could assist these vehicles to calculate the available grip on a road surface and thus the corresponding safety distances to be left between other vehicles. Of course, for such applications, it will be necessary to equip these cars with additional sensors capable of collecting data from the surrounding environment (a profilometer in front of the tires, a sensor to detect the contaminant and its characteristics, a piezo sensor to measure load variations …).

Other future applications could be for road builders to assist them to achieve the right texture to meet the required surface performances. Tire manufacturers could also use the tool in the future to optimize rubber materials from the development phases of new tires with simulations instead of undertaking expensive tests.

7. CONCLUSION

This paper presented the development of a tool to estimate tire/road friction. This tool rigorously takes into account all parameters related to tire, road, and contact operating conditions. For the tire, it takes into account its geometries and rubber material and tread patterns. For the road, it takes into account the surface texture and contaminant conditions via the lubricant depth, viscosity, and density. The operating conditions are taken into account via the load, speed, and slip ratio of the tire.

The tool is validated by performing braking tests with a passenger vehicle at different speeds on wet roads of different textures. Even there are still areas of improvement, the trend of the results predicted was similar to those obtained in experiments.

8. ACKNOWLEDGMENT

I would like to thank the Tire Technology Expo 2020 conference where the software derived from the work presented here has been introduced (Malal Kane (2020, February 25-27). Tire/road friction: a skid resistance tool based on contact modeling) and confirm that the conference paper is not published anywhere else.

9. REFERENCES

[1] Kane, M.., Scharnigg, K., Factors affecting parameters of tyre/road contact: skid resistance, noise emission and rolling resistance, Deliverable 10, TYROSAFE (Tyre and Road Surface Optimisation for Skid resistance and Further Effects), EU, PCRD, FP7/2007-2013, Juillet 2009

[2] D. F.Moore, Friction and wear in rubbers and tyres, Wear, Volume 61, Issue 2, 16 June 1980, Pages 273-282,https://doi.org/10.1016/0043-1648(80)90291-4

[3] Tabor, D., Giles, C. G., and Sabey, B. E., "Friction between Tyre and Road: Hysteresis Loss in the Friction of Lubricated Rubber; Rubber Hysteresis and Skidding Resistance," Engineering, 1958, Vol. 186, No. 4842, pp.

[4] Heinrich, G. (1997) Hysteresis Friction of Sliding Rubbers on Rough and Fractal Surfaces. Rubber Chemistry and Technology: March 1997, Vol. 70, No. 1, pp. 1-14. https://doi.org/10.5254/1.3538415

[5] Villani, M., Artamendi, I., Kane, M., Scarpas, A., Contribution of hysteresis component of tire rubber friction on stone surfaces, (2011) Transportation Research Record, (2227), pp. 153-162., DOI: 10.3141/2227-17

[6] W. E. Meyer, Frictional Interaction of Tire and Pavement, ASTM, 1983, 334 pages

[7] Wong, J. Y., Theory of Ground Vehicles, 4th Edition | Wiley, ISBN: 978-0-470-17038-0 August 2008 592 Pages

[8] Al-Assi, M., Kassem, E., Evaluation of Adhesion and Hysteresis Friction of Rubber–Pavement System, Appl. Sci. 2017, 7(10), 1029; https://doi.org/10.3390/app7101029

[9] ISO 13473-2:2002, Characterization of pavement texture by use of surface profiles - Part 2: Terminology and basic requirements related to pavement texture profile analysis, by ISO/TC 43/SC 1

[10] Sabey B.E., 1958, Pressure Distribution beneath Spherical and Conical Shapes Pressed into a Rubber Plane, and their Bearing on Coefficient of Friction under Wet Conditions, Proceedings of the Physical Royal Society, Vol.71, pp 979-988.

[11] Leu, M.C., Henry, J.J., 1983. Prediction of Friction as a Function of Speed from Pavement Texture. Transportation Research Record, No. 946, Transportation Research Board, Washington, DC.

[12] Fwa T.F., Friction determination for pavement management and wet-weather road safety, International Journal of Transportation Science and Technology, Volume 6, Issue 3, September 2017, Pages 217-227

[13] ASTM: Calculating International Friction Index of a Pavement Surface, Standard No.E1960-98, ASTM 1998

[14] Kulakowski B T., Mathematical Model of Friction as a Function of Speed, Transportation Research Board, Issue Number: 1311, p. 26-33, 1991

[15] Sabey, B. E., Williams, T. E. and Lupton, G. N.,"Factors Affecting the Friction of Tires on Wet Roads," SAE Paper No. 700376, 1970 International Automobile Safety Conference Compendium, pp. 324-340, 1970

[16] Srirangam, S.K., Anupam, K., Scarpas, A., Kasbergen, C., Kane, M., Safety aspects of wet asphalt pavement surfaces through field and numerical modeling investigations, (2014) Transportation Research Record, 2446, pp. 37-51. , DOI: 10.3141/2446-05

[17] Dugoff, H., Fancher, P., and Segel, L., "An Analysis of Tire Traction Properties and Their Influence on Vehicle Dynamic Performance," SAE Technical Paper 700377, 1970, doi:10.4271/700377

[18] Kiencke U., Daiss A. "Estimation of Tyre Friction for Enhanced ABS Systems". Proceedings of the AVEC'94, 1994

[19] Bian, M., Chen, L., Luo, Y., and Li, K., "A Dynamic Model for Tire/Road Friction Estimation under Combined Longitudinal/Lateral Slip Situation," SAE Technical Paper 2014-01-0123, 2014, doi:10.4271/2014-01-0123

[20] Pacejka H. B., "Tyre and Vehicle Dynamics", Butterworth-Heinemann, UK, 2006. Canudas-de-Wit Carlos, Tiotras Panagiotis, Velenis Efstathios, and Basset Michel, et al., "Dynamic Friction Models for Road/Tire Longitudinal Interaction," Vehicle System Dynamics, 39(3):189-226,2003

[21] Faria, L.O., Oden, J.T., Yavari, B.T., Tworzydlo,W.W., Bass, J.M. and Becker, E.B.: Tire Modeling by Finite Elements. Tire Science and Technology 20(1) (1992), pp. 33–56.

[22] Piatkowski T., Dahl and LuGre dynamic friction models — The analysis of selected properties, Mechanism and Machine Theory, Volume 73, March 2014, Pages 91-100

[23] Carlos Canudas-de-Wit, Panagiotis Tsiotras, Efstathios Velenis, Michel Basset & Gerard Gissinger (2003) Dynamic Friction Models for Road/Tire Longitudinal Interaction, Vehicle System Dynamics, 39:3, 189-226, DOI: 10.1076/vesd.39.3.189.14152

[24] Persson, B. N. J. Theory of rubber friction and contact mechanics, J. Chem. Phys. 115, Issue 8, 3840, 22p. 2001

[25] Motamedi, Mohammad. "Road Surface Measurement and Multi-Scale Modeling of Rubber Road Contact and Adhesion." (2015).

[26] Kane, M., Do, M.-T., Cerezo, V., Rado, Z., Khelifi, C., Contribution to pavement friction modelling: an introduction of the wetting effect, (2017) International Journal of Pavement Engineering, 20 (8), pp. 965-976. , DOI: 10.1080/10298436.2017.1369776

[27] Scaraggi, M. and B. Persson, Theory of viscoelastic lubrication. Tribology International, 2014. 72: p. 118-130.

[28] Bérengier, M., Cesbron, J., Klein, Ph., Béguère, A., Conte, F., Tian, B., Palhevani, L., Duhamel, D., Wang, B., Pouteau, B., and Coquelle, E., Odsurf : Modélisation et réalisation d'une couche de roulement de chaussée optimisée, dense et peu bruyant. Technical report, ADRME 11 17 C0038 213 pages, 2016

[29] Delanne, Y., Gothié, M., Influence de l'état de mouillage sur les performances d'adhérence des pneumatiques, BULLETIN DES LABORATOIRES DES PONTS ET CHAUSSÉES – 255, 2005 - RÉF. 4564 - PP. 23-34

[30] Book, "Specification for a standard test tyre for friction coefficient measurement of a pavement surface: ribbed test tyre", Date: 2009, Author(s): Comité technique 1 Caractéristiques de Surface / Technical Committee 1 Surface Characteristics, PIARC Ref. : 2009R03EN, Number of pages: 23, ISBN : 2-84060-223-7